Substorm simulation: Insight into the mechanisms of initial brightening

AUTHOR(S):

Ebihara, Y.; Tanaka, T.

CITATION:

Ebihara, Y. ...[et al]. Substorm simulation: Insight into the mechanisms of initial brightening. Journal of Geophysical Research: Space Physics 2015, 120(9): 7270-7288

ISSUE DATE:

2015-09

URL:

http://hdl.handle.net/2433/203274

AGU PUBLICATIONS
JGR
Journal of Geophysical Research: Space Physics

RESEARCH ARTICLE
10.1002/2015JA021516

Key Points:
- Initial brightening of aurora at substorm expansion onset is investigated by MHD simulation
- High-pressure region moves earthward along a field line after flow braking near equatorial plane
- Upward field-aligned current is generated by vortex in the off-equatorial high-pressure region

Supporting Information:
- Figure S1

Correspondence to:
Y. Ebihara,
ebihara@rish.kyoto-u.ac.jp

Citation:
Ebihara, Y., and T. Tanaka (2015), Substorm simulation: Insight into the mechanisms of initial brightening, *J. Geophys. Res. Space Physics*, *120*, 7270–7288, doi:10.1002/2015JA021516.

Received 3 JUN 2015
Accepted 9 AUG 2015
Accepted article online 13 AUG 2015
Published online 9 SEP 2015

Substorm simulation: Insight into the mechanisms of initial brightening

Y. Ebihara[1] and T. Tanaka[2]

[1]Research Institute for Sustainable Humanosphere, Kyoto University, Uji, Japan, [2]International Center for Space Weather Science and Education, Kyushu University, Fukuoka, Japan

Abstract Initial brightening of the aurora is an optical manifestation of the beginning of a substorm expansion and is accompanied by large-amplitude upward field-aligned currents (FACs). Based on global magnetohydrodynamic simulation, we suggest the possible generation mechanism of the upward FAC that may manifest the initial brightening. (1) A formation of the near-Earth neutral line (NENL) releases the tension force that accelerates plasma earthward. (2) The earthward (perpendicular) flow is converted to a field-aligned flow when flow braking takes place. (3) A high-pressure region propagates earthward along a field line. (4) The off-equatorial high-pressure region pulls in and discharges ambient plasma, which generates a flow vorticity around it. (5) Region 1-sense FAC is generated in the upper part of the off-equatorial high-pressure region. (6) The upward FAC is connected with the ionosphere in the center of the Harang discontinuity, causing the initial brightening. Additional dynamo is generated in the near-Earth region, which transmits electromagnetic energy. Upward FAC that manifests the initial brightening seems to be necessarily originated in the near-Earth off-equatorial region where the magnitude of the perpendicular (diamagnetic) current is relatively small in comparison with that of the FAC. Near the equatorial plane, the perpendicular current is comparable to or larger than FAC so that a current line is diverted from a magnetic field line and that the FAC generated near the equatorial plane is not necessarily connected with the ionosphere. The proposed mechanism occurs regardless of the location of the NENL and may explain some of auroral forms.

1. Introduction

The expansion phase of an auroral substorm begins with a sudden brightening of a quiet evening arc (QEA). This initial brightening of the aurora lasts for a few minutes, followed by rapid poleward and westward motions [*Akasofu*, 1964]. The initial brightening occurs within the region where protons (>1 keV) and electrons (>40 keV) are precipitating, which suggests that the initial brightening takes place on closed field lines [e.g., *Lui and Burrows*, 1978; *Samson et al*., 1992; *Kadokura et al*., 2002; *Mende et al*., 2003; *Yago et al*., 2007]. According to statistical studies, the initial brightening of the aurora during the expansion phase occurs preferentially in the premidnight sector [*Elphinstone et al*., 1995; *Liou et al*., 2001; *Deehr and Lummerzheim*, 2001]. After the initial brightening, the expansion phase undergoes a two-step or multi-step evolution during substorm development [*Sergeev and Yahnin*, 1979; *Rostoker et al*., 1987; *Craven et al*., 1989; *Kadokura et al*., 2002; *Saito et al*., 2010]. For example, *Saito et al*. [2010] presented global auroral images taken by the Polar satellite during substorm expansion, to show that the auroral evolution is spatially and temporally separable into two periods of intense auroral activities, which were separated by 4.5 min.

Ground-based magnetometer data show that additional current vortices appear at or soon after the onset of the auroral substorm (hereinafter referred to as "onset") on the nightside [*Untiedt and Baumjohann*, 1993; *Kamide et al*., 1996; *Lyatsky et al*., 2001; *Weygand et al*., 2008; *Keiling et al*., 2009]. Clockwise and counterclockwise rotations of the ionospheric Hall currents are identified on the dawnside and duskside, respectively, suggesting the existence of a pair of downward and upward field-aligned currents (FACs) that have a sense equivalent to Region 1 FACs. The newly appearing upward FAC is thought to be related to the initial brightening of the aurora at the onset of the expansion. Traditionally, a pair of Region 1-sense FACs has been understood in terms of a current wedge, in which the dawn-to-dusk cross-tail current is diverted from the equatorial plane to the ionosphere [*McPherron et al*., 1973; *Kepko et al*., 2014, and references therein]. The current wedge has been suggested to form in the near-Earth region and spread tailward [*Lopez and Lui*, 1990], longitudinally [*Nagai*, 1982; *Lopez and Lui*, 1990], and earthward [*Ohtani*, 1998]. A number of mechanisms have been proposed for the generation of this pair of Region 1-sense FACs, including current disruption

[*Lui*, 1996], dawnward inertial currents [*Shiokawa et al*., 1997], pressure gradients [*Shiokawa et al*., 1998; *Birn et al*., 1999; *Yao et al*., 2012], flow vortices near the equatorial plane [*Birn et al*., 2004; *Keiling et al*., 2009], and low-entropy magnetic flux tubes (or plasma bubbles) [*Sergeev et al*., 1996; *Chen and Wolf*, 1999; *Nakamura et al*., 2001; *Birn et al*., 2004; *Xing et al*., 2011].

Many explanations for the generation of the current wedge are based on the current continuity condition derived from the force balance equation [*Hasegawa and Sato*, 1979; *Sato and Iijima*, 1979; *Vasyliunas*, 1984]. However, *Song and Lysak* [2001a, 2001b] pointed out that the current continuity condition may be insufficient for understanding FAC generation [*Song and Lysak*, 2001a, 2001b]. First, one must also discuss the effect of the induction equation on the generation of FAC in terms of $\partial J_{||}/\partial t$, where $J_{||}$ is FAC. From the Ampère and Faraday laws, the generation of FAC is given by

$$\frac{\partial J_{||}}{\partial t} = -\frac{1}{\mu_0}(\nabla\times\nabla\times\mathbf{E})_{||}, \tag{1}$$

where **E** is the electric field and μ_0 is the magnetic constant. When perturbations start with an initially uniform magnetic field, the following approximation is also used [*Paschmann et al*., 2002]:

$$\frac{\partial J_{||}}{\partial t} = \frac{1}{\mu_0}\mathbf{B}\cdot\nabla\Omega_{||}, \tag{2}$$

where $\Omega_{||} = \mathbf{B}\cdot(\nabla\times\mathbf{V})/B$, **B** is the magnetic field, and **V** is the plasma velocity. Second, to understand the process of $\partial J_{||}/\partial t$, one must discuss the generation of $\Omega_{||}$ [*Song and Lysak*, 2001b; *Paschmann et al*., 2002] in terms of force balance. Third, since the ionosphere is a load (a sink for electromagnetic energy), there must be a dynamo in the magnetosphere to supply electromagnetic energy to the ionosphere. According to the Poynting theorem, a source or sink for electromagnetic energy is given by the following equation:

$$\nabla\cdot\left(\frac{\mathbf{E}\times\mathbf{B}}{\mu_0}\right) = -\mathbf{J}\cdot\mathbf{E} - \frac{\partial}{\partial t}\left(\frac{B^2}{2\mu_0}\right). \tag{3}$$

One must discuss the region in the magnetosphere where either the first term or the second term of the right-hand side of equation (3) is positive.

Birn and Hesse [2005] suggested that an off-equatorial dynamo region is generated in the plasma sheet during the expansion phase and that this dynamo is associated with flow vorticities causing the Region 1-sense FAC. The two terms on the right-hand side of equation (3) contribute about equally to the generation of the electromagnetic energy. *Haerendel* [2010] pointed out that stretched magnetic field lines exert a force accelerating the plasma from the highly stretched region to the dipolar magnetic field region. The plasma is squeezed out, and an extended plasma layer is formed earthward of the inner edge of the plasma sheet. This extended layer is suggested to generate the electromagnetic energy.

Using an advanced global magnetohydrodynamics (MHD) simulation, Tanaka (Substorm auroral dynamics reproduced by the advanced global M-I coupling simulation, in Auroral Dynamics and Space Weather, AGU Monogr., ed. Y. Zhang, in press) discussed the origin of Region 1 and Region 2 FACs in the magnetosphere-ionosphere coupling system during the growth and expansion phases. During the growth phase, an upward FAC that is elongated longitudinally does appear in the evening sector, which is referred to as a QEA. Magnetic field lines extending from the equatorward part of the QEA are closed, whereas those extending from the poleward part are open. Although starting from same points, current lines deviate from the magnetic field lines and go through the lobe-plasma sheet boundary by way of the high-latitude side of the cross-tail current. They finally reach the cusp-mantle region that acts as a dynamo for the QEA. The FAC related to the QEA is guided by flow shear near the transition layer between the lobe and the plasma sheet. After the formation of a near-Earth neutral line (NENL) [*Nishida and Nagayama*, 1973], magnetic tension released from the NENL propagates earthward to enhance the plasma pressure in the inner magnetosphere near midnight. This process is referred to as dipolarization. A spatially compact dynamo forms in the near-Earth, high-latitude region (near-Earth dynamo) at the early stage of the dipolarization, which is a direct cause for the onset of the substorm. Plasma pressure increases in the inner magnetosphere, and this high-pressure region expands longitudinally. The near-Earth dynamo continues to form at the leading edge of the expanded high-pressure region, which generates the upward FAC moving westward together with the near-Earth dynamo. This is referred to as westward traveling surge. These results indicate that convection is strongly coupled with the FACs and that the FACs must be understood in terms of force balance, dynamo,

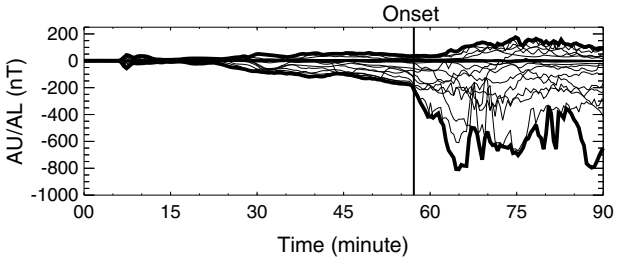

Figure 1. *H* component of the magnetic field disturbance on the ground at different 24 MLTs at magnetic latitude of 67°. The upper and lower envelopes of the superposed plots correspond to the AU and AL indices, respectively. The vertical line indicates the substorm expansion onset determined by the sudden intensification of the upward field-aligned current near midnight.

and shear. The purpose of this study is to analyze the generation of the initial brightening and associated FACs in more detail to clarify the roles that dynamo and shear play in this process.

We admit that a MHD simulation cannot deal with microscopic and kinetic processes such as kinetic cross-field streaming instability [*Lui et al*., 1990] and kinetic ballooning instability [*Cheng and Lui*, 1998]. Because of current limitations of computational resources, a full Vlasov simulation cannot cover the entire domain from the solar wind to the inner magnetosphere. However, a MHD simulation provides a solution that fully satisfies continuity of mass, momentum, energy, force balance, and Faraday's and Ampère's laws throughout the domain from the solar wind to the inner magnetosphere. Recently obtained results using a high-resolution grid system show that many of the striking features associated with substorms are global in nature and can be represented by MHD equations [*Tanaka et al*., 2010; *Ebihara and Tanaka*, 2013; *Ebihara et al*., 2014].

2. Simulation

We used the MHD simulation developed by Tanaka (Substorm auroral dynamics reproduced by the advanced global M-I coupling simulation, in Auroral Dynamics and Space Weather, AGU Monogr., ed. Y. Zhang, in press). The ionosphere is coupled with the magnetosphere in two ways. First, we calculated the height-integrated ionospheric conductivity tensor by using FACs and the plasma pressure mapped from the inner boundary of the magnetosphere domain (at a geocentric distance of 2.6 Re for this particular study). Solving an elliptic partial differential equation for the given FAC and ionospheric conductivity, we obtained the electric potential at the ionosphere altitude [e.g., *Tanaka*, 1994]. The electric field is fed back to the inner boundary of the magnetosphere domain. The MHD simulation does not solve kinetic equations for precipitating electrons and the associated excitation processes of atoms and molecules in the thermosphere. Instead, we introduced empirical equations that relate the FAC and plasma pressure to the height-integrated conductivity. The ionospheric conductivity used in this study is described by *Ebihara et al*. [2014] in detail.

In order to illuminate the essence underlying the evolution of auroral structures, we imposed a simple step function at the simulation boundary upstream in the solar wind. The *Z* component of the interplanetary magnetic field (IMF) was changed from +5 nT to −5 nT, and the solar wind speed was increased from 372 to 500 km s^{-1}. The solar wind density and *Y* component of the IMF were kept constant at 5 cm^{-3} and 2.5 nT, respectively. All simulation settings, grid system, and ionospheric conductivities are the same as those used by *Ebihara et al*. [2014]. The grid system is based on a dodecahedron [*Moriguchi et al*., 2008]. The inner surface is divided into 12 pentagons. Each pentagon is divided into five triangles. We call this Level 1. Furthermore, we divide each triangle into four. We call this Level 2. We used Level 6, in which a sphere is divided into 61,440 triangles. Triangular prisms are stacked from the inner boundary outward. To concentrate grid points near the equatorial plane on the nightside, the direction of the stacking is skewed. The grid spacing in the outward direction is 0.044 Re at 2.6 Re, and 0.22 Re at 12 Re at midnight in the equatorial plane. Readers may refer to *Ebihara et al*. [2014] and Tanaka (Substorm auroral dynamics reproduced by the advanced global M-I coupling simulation, in Auroral Dynamics and Space Weather, AGU Monogr., ed. Y. Zhang, in press) for more detailed information about the simulation settings, grid system, and ionospheric conductivities.

3. Results

Figure 1 shows the AU and AL indices calculated based on the *H* component of magnetic disturbances at 24 different magnetic local times (MLTs) and a magnetic latitude (MLAT) of 67°. The azimuthal component of the ionospheric Hall current was used to calculate the magnetic disturbances. Changes in solar wind velocity and

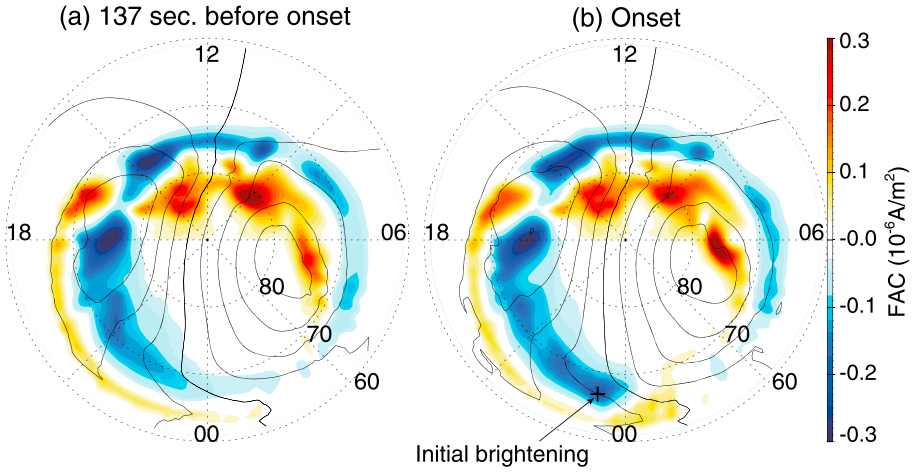

Figure 2. Field-aligned currents (FACs) at the ionosphere altitude (a) at 137 s before the onset ($t = 55.05$ min) and (b) at onset ($t = 57.34$ min). Negative value (blue color) indicates upward FAC. The contour lines indicate the ionospheric electric potential. Sun is to the top. The plus sign (+) denotes the most intensified upward FAC at onset.

IMF arrive at the magnetosphere and disturb the AU and AL indices at $t \approx 6$ min. Subsequently, the growth phase progresses, which can be identified by a gradual decrease in the AL index. At $t \approx 57$ min, AL shows a rapid decrease because of rapid intensification of the westward electrojet in the ionosphere. For this particular study, we identified the onset of the substorm expansion based on the sudden intensification of the upward FAC near midnight to $t = 57.34$ min. The onset is marked by a vertical line in Figure 1.

Figure 2 shows the FACs at ionosphere altitude at $t = 55.05$ min (137 s before the onset) and at $t = 57.34$ min (onset). Large-scale FACs, which are consistent with those known as Region 1 and 2 current systems [*Iijima and Potemra*, 1976], are clearly visible. In the left panel, the upward FAC that occupies the midnight-dusk sector can be regarded as a source of a quiet evening arc (QEA) [e.g., *de la Beaujardiere et al*., 1977; *Marklund et al*., 1982; *Aikio et al*., 2002; *Marghitu et al*., 2009]. Optical observations have shown that the thickness of each QEA ranges from a few hundred meters to several tens of kilometers in latitude, which is much thinner than that of the upward FAC [*Paschmann et al*., 2002]. The reason for this difference is that auroral arcs are embedded in a single layer of a large-scale upward FAC and that each FAC layer does not always correspond to each arc [*Stenbaek-Nielsen et al*., 1998; *Marghitu et al*., 2009; *Fukuda et al*., 2014]. At $t = 57.34$ min (right panel), the upward FAC is suddenly intensified at 66.7 MLAT and 2318 MLT, which is denoted by a plus sign (+). Hereinafter, we call it initial intensification of the upward FAC and regard it as an initial "brightening" of the aurora, simply called initial brightening. Contour lines show the electric potential at ionosphere altitude. The initial brightening occurs in a region where the electric potential lines are skewed toward the east, which is known as the Harang discontinuity [*Heppner*, 1972]. This is consistent with observations that most of the onset of substorm expansion takes place in the vicinity of the Harang discontinuity or a similar vortex of ionospheric current [e.g., *Nielsen and Greenwald*, 1979; *Untiedt and Baumjohann*, 1993; *Lyatsky et al*., 2001; *Weygand et al*., 2008; *Zou et al*., 2009].

Figure 3 summarizes the FAC and the ionospheric conductivity as a function of MLAT and time at 2318 MLT. During the growth phase, the large-scale upward FAC (which may correspond to a QEA) and the high-conductivity region move equatorward. At onset, indicated by a vertical line, the upward FAC starts to intensify at 66.7 MLAT and expands poleward and equatorward. The sudden intensification of the upward FAC (initial brightening) occurs in the equatorward part of the preexisting upward FAC (which may be associated with a QEA).

Figure 4 shows a temporal sequence of the X component of the plasma flow V_x and the plasma pressure P at midnight. Before the onset, the NENL had formed at $X \approx -12$ Re, which resulted in an earthward acceleration of plasma (Figure 4, M1 and M2). The plasma was then squeezed out, and a high-pressure region formed in the inner magnetosphere (Figure 4, M3). This process was already pointed out by *Haerendel* [2010] and *Tanaka et al*. [2010]. The plasma is then decelerated by the plasma pressure and magnetic pressure forces (Figure 4, M4), which results in compression of plasma and enhancement of the plasma pressure

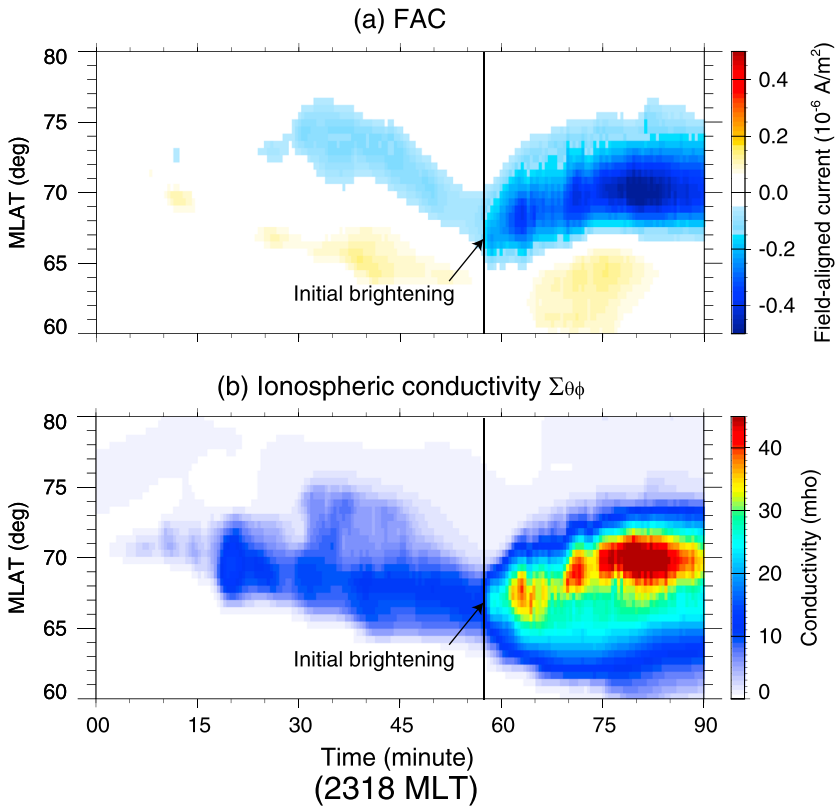

Figure 3. (a) Field-aligned current (negative upward) and (b) nondiagonal component of the ionospheric conductivity as a function of magnetic latitude (MLAT) and time at 2318 MLT. A vertical line indicates the substorm expansion onset determined by the initial intensification of the field-aligned current.

near the equatorial plane (Figure 4, M5) just outside the high-pressure region associated with squeezing (Figure 4, M3). This is consistent with the result of a simulation performed by *Birn et al.* [2004] and *Tanaka et al.* [2010]. Thus, there are two pressure peaks near the equatorial plane. The plasma pressure is the highest near the equatorial plane, giving rise to a pressure gradient along a field line, which accelerates plasma toward Earth along this field line. A portion of the high-pressure region moves earthward along a field line (Figure 4, M7), hereinafter called an off-equatorial high-pressure region. We have to note first that motion of the off-equatorial high-pressure region does not necessarily represent that of plasma element. Plasma element can move earthward along a field line even though the off-equatorial high-pressure region is stationary. Second, since the boundary condition allows plasma to flow freely through the inner boundary, plasma may escape from the magnetosphere rapidly. This may imply that the off-equatorial high-pressure region would be smaller in magnitude and shorter in time in comparison with the real magnetosphere. Thus, this simulation may provide the lower limit of the structure and the intensity of the off-equatorial high-pressure region. The generation of the parallel flow and temporal sequence of the off-equatorial high-pressure region were described by *Birn et al.* [2004] and *Tanaka et al.* [2010] in more detail. Third, the NENL has been observed at ≈20 to 30 Re [*Nagai et al.*, 1998; *Angelopoulos et al.*, 2008]. *Sergeev et al.* [2008] found unusual events that occurred at ≈9 to 13 Re. The location of the NENL is highly variable depending on parameters assumed. However, after running many simulations with different parameters, we carefully confirmed that the results presented in this paper are essentially the same regardless of the location of the NENL ranging between ≈12 Re and ≈40 Re.

Figure 5 summarizes the X component of the plasma velocity V_x, the parallel vorticity $\Omega_{||}$, and the plasma pressure in the equatorial plane. The earthward fast flow is maximized around $X \approx -8$ Re (Figure 5, M1). Flow shear is generated in the western (eastern) part of the earthward fast flow, resulting in positive (negative) $\Omega_{||}$ on the duskside (Figure 5, M2). The vorticity generates the Region 1-sense FAC near the equatorial plane. The plus sign (+) indicates the point where the magnetic field line extending from the initial

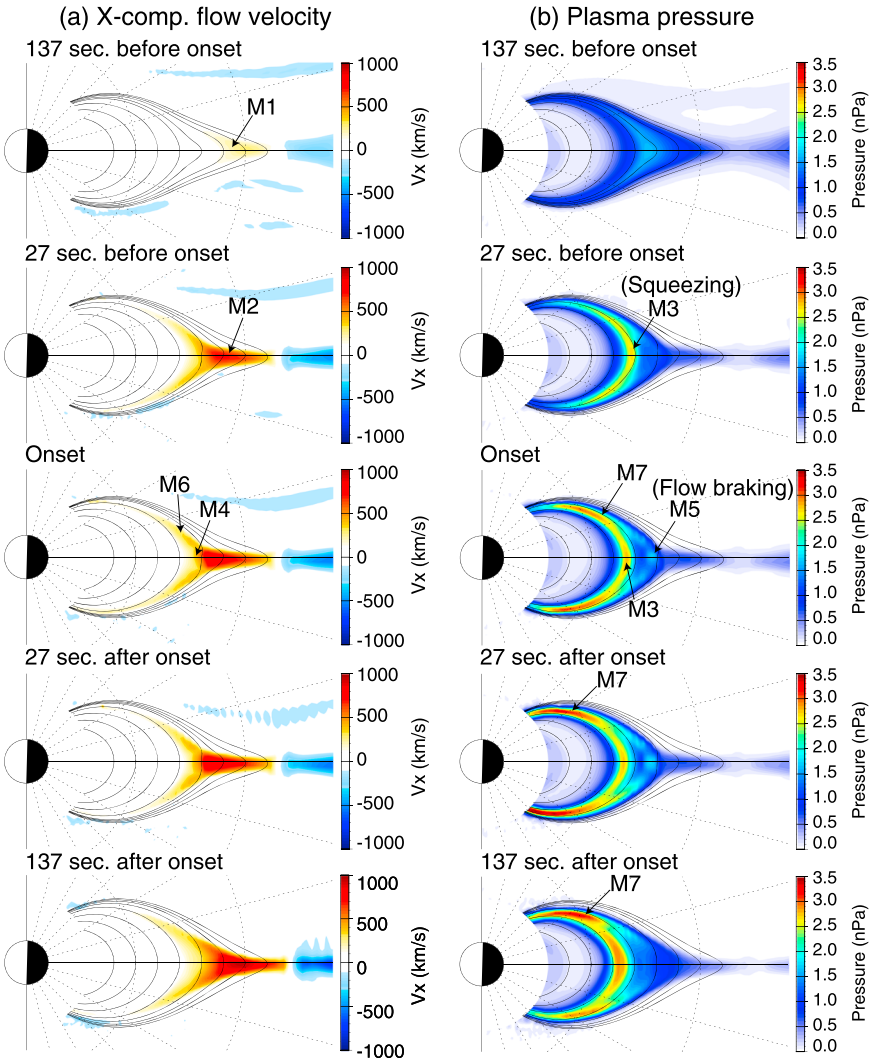

Figure 4. (a) *X* component of plasma flow velocity V_x and (b) plasma pressure at midnight. Sun is to the left. The black lines indicate magnetic field lines. The inner and outer circles indicate the radial distance of 5 Re and 10 Re, respectively.

brightening intersects the equatorial plane. That is, the plus sign in Figure 2b is a magnetic footprint of the plus sign in Figure 5b. It is found that the initial brightening is not connected by a magnetic field line with the strongest $\Omega_{||}$ in the equatorial plane (Figure 5, M2). We also shifted time to take into account the Alfvén transit time, which led to essentially the same result. The bottom panel of Figure 5 shows the plasma pressure. At the onset, there are two peaks. The inner peak (Figure 5, M3) is primarily caused by squeezing of the plasma [*Haerendel*, 2010; *Tanaka et al.*, 2010], while the outer peak (Figure 5, M4) is primarily caused by flow braking [*Birn et al.*, 2004; *Tanaka et al.*, 2010].

Figure 6 shows a snapshot of current lines and magnetic field lines at onset of the substorm expansion. The magnetic field lines (white lines) are drawn from the region where $\Omega_{||} > 0.1\ s^{-1}$ in the equatorial plane (Figure 5, M2). The magnetic field lines reach the ionosphere close to the area of initial brightening (several to ~10° east of the initial brightening). We also drew current lines (I) from the region where $\Omega_{||} > 0.1\ s^{-1}$ in the equatorial plane (Figure 5, M2). Because of the presence of $\Omega_{||}$ near the equatorial plane, downward and upward FACs are generated in the postmidnight and premidnight regions, respectively. Due to the field-aligned component of the current, current lines (I) deviate from the equatorial plane. The shape of current lines (I) resembles that known as a current wedge [e.g., *McPherron et al.*, 1973]. However, current lines (I) are not connected with the ionosphere because the current line is diverted by the strong diamagnetic current ($\mathbf{J}_\perp = \mathbf{B} \times \nabla P/B^2$) that surrounds the secondary pressure peak

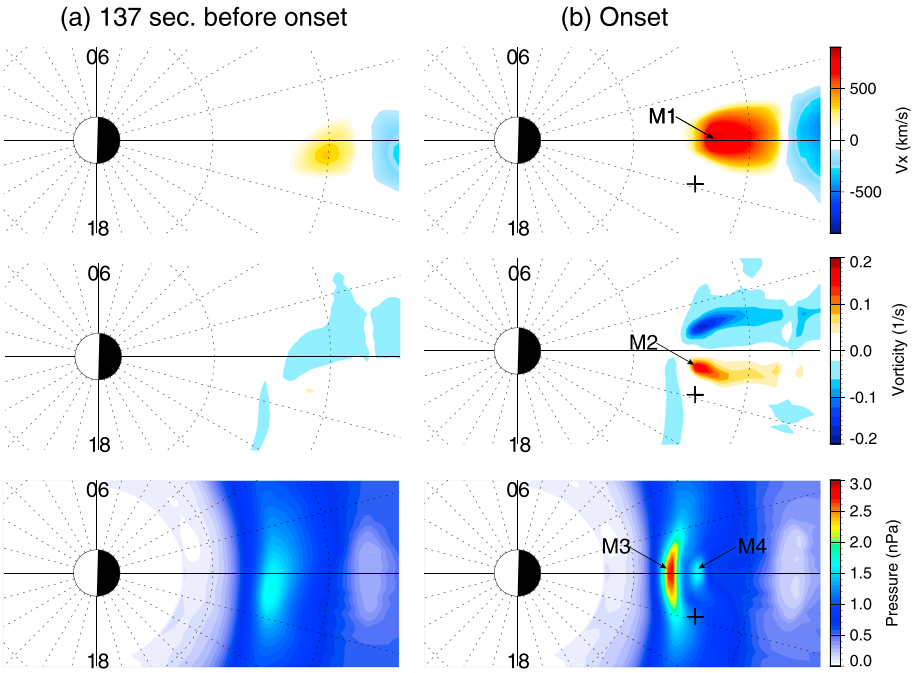

Figure 5. (top) *X* component of the plasma velocity V_x, (middle) the vorticity parallel to the magnetic field line, and (bottom) the plasma pressure in the equatorial plane (a) at 137 s before the onset ($t = 55.05$ min) and (b) at onset ($t = 57.34$ min). The inner and outer circles indicate the radial distance of 5 Re and 10 Re, respectively.

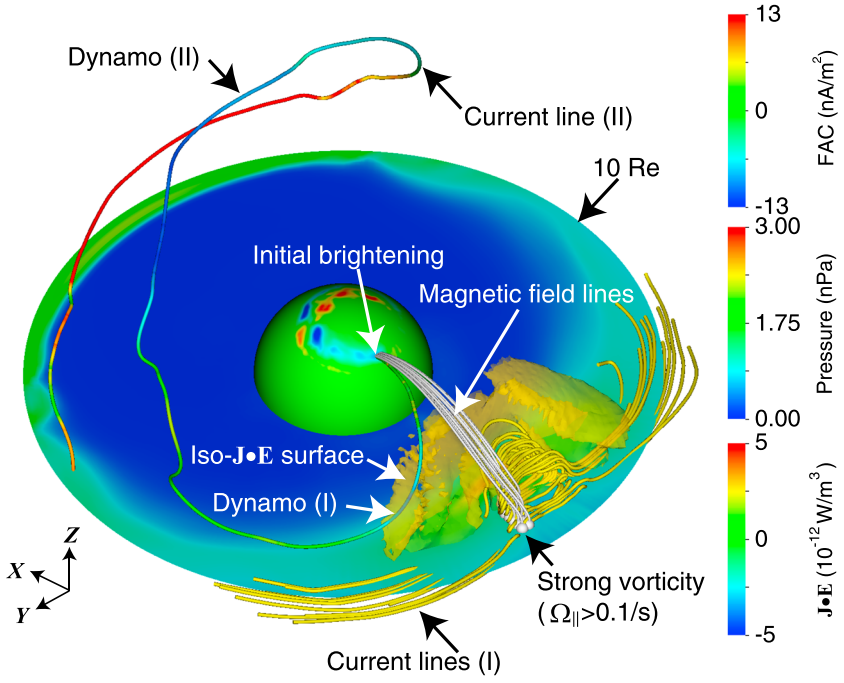

Figure 6. Snapshot of current lines and magnetic field lines at onset ($t = 57.34$ min). Magnetic field lines and current lines (I) are extended from the region where $\Omega_{||} > 0.1\ s^{-1}$ in the equatorial plane. Current line (II), colored with the value of **J•E**, is extended from the initial brightening. The yellowish surface is an iso-**J•E** surface at $-2.3\ 10^{-12}\ Wm^{-3}$, that is, a dynamo region. Color codes drawn in the equatorial plane indicate the plasma pressure, and color codes drawn in the sphere (with a radius of 3 Re) indicate the field-aligned current.

(Figures 4, M5, and 5, M4). We call this an incomplete current wedge because the leg of the current wedge is too short to reach the ionosphere (inner boundary of the simulation). The same result was obtained when we traced the current lines starting in a wide area in the equatorial plane (Figure S1 of the supporting information).

To investigate the origin of the FAC that manifests the initial brightening, we present current line (II) that extends from the point of initial brightening. The color code of current line (II) indicates the value of **J**•**E**. Current line (II) is diverted westward by the diamagnetic current and is connected with the high-latitude mantle region where $\mathbf{J}\cdot\mathbf{E} < 0$. An interesting feature to note is that the initial brightening is not connected by a current line with the equatorial plane.

There are two regions where $\mathbf{J}\cdot\mathbf{E} < 0$ along current line (II). One is located just above the equatorial plane as denoted by Dynamo (I). The yellowish surface is the iso-**J**•**E** surface at $-2.3\ 10^{-12}$ W m^{-3} and implies a dynamo region. (The surface is present only on the nightside.) Dynamo (I) is distributed longitudinally but is confined near the equatorial plane. Dynamo (I) is associated with the inner high-pressure region (Figure 5, M3) that is caused by squeezing of plasma [*Haerendel*, 2010]. The other dynamo is located in the high-latitude mantle region as denoted by Dynamo (II). Dynamo (II) exists for the southward IMF regardless of the phase of the substorm [*Tanaka et al*., 2010]. Thus, Dynamo (I) is thought to play a role in generating the electromagnetic energy associated with the initial brightening.

In Figure 7, pressure, parallel vorticity $\Omega_{||}$, $\partial J_{||}/\partial t$, FAC, magnitude of the perpendicular current, and angle between **J** and **B** taken along the magnetic field line that passes through the westward edge of the incomplete current wedge are shown. In each panel, the ordinate is the distance along the field line toward the Earth. The distance 0 corresponds to the equatorial plane (−7.60, 0.98, 0.0) Re. The farthest distance corresponds to the radial distance of 4 Re. The magnetic footprint of this field line is located at 67.2 MLAT and 2336 MLT at onset. Before the onset, the plasma pressure has increased, and the high-pressure region moves earthward (Figure 7, M1). Positive vorticity and the upward FAC ($\partial J_{||}/\partial t<0$) are generated (Figure 7, M2 and M3). The upward FAC ($J_{||} < 0$) appears almost entirely along the field line. Near the equatorial plane, the upward FAC is not clearly generated on this field line (Figure 7, M4). In general, the magnitude of the perpendicular current is large except at the distance of 1.2 Re (Figure 7, M5). At this point, the FAC dominates the perpendicular current so that the current density vector is almost antiparallel to the magnetic field line (Figure 7, M6). The antiparallel current density (upward FAC) is a part of the short leg of the incomplete current wedge shown in Figure 6. In general, **J** is not always aligned with **B**. The angle between them is sometimes less than 150° when the perpendicular current is large (Figure 7, M7). This implies that even though the FAC is generated along a field line, the current line will be easily diverted from the magnetic field line because of the existence of the perpendicular current.

Figure 8 summarizes $PV_{||}$, pressure, number density, parallel vorticity $\Omega_{||}$, $\partial J_{||}/\partial t$, FAC, and angle between **J** and **B** taken along a magnetic field line extending from the location of the initial brightening in the ionosphere (the plus sign in Figure 2). In each panel, the ordinate is the distance along a field line toward the equatorial plane. The distance 0 corresponds to (−3.2, 0.6, 2.3) Re (which is the geocentric distance of 4.0 Re). The farthest distance corresponds to the equatorial plane. The ordinate is opposite to that of Figure 7. The solid curve indicates the propagation of the shear Alfvén wave calculated based on the local Alfvén speed. Just before the onset, the high-pressure region moves earthward along a field line (Figure 8, M1). The number density of plasma is larger at a small distance near the onset (Figure 8, M2). The strong positive $\Omega_{||}$ region (Figure 8, M3) also propagates earthward. The magnitude of parallel vorticity decreases with decreasing distance (Figure 8, M4) because the number density of plasma is larger at lower distance (Figure 8, M2). Dense plasma (large mass density) causes acceleration to be small for given inertial forces. The generation of inertial forces will be mentioned below. The upward FAC is generated ($\partial J_{||}/\partial t < 0$) near the earthward edge of the high vorticity region (Figure 8, M5). As the strong positive $\Omega_{||}$ region moves earthward (Figure 8, M3), the strong upward FAC region also moves earthward (Figure 8, M6). When the strong upward FAC region arrives at the lowest distance (distance of 0), the initial brightening takes place in the ionosphere. The integral of $\partial J_{||}/\partial t$ with respect to time is not equal to $J_{||}$. Probable reasons for this behavior are that the generated FAC immediately propagates along a field line as a shear Alfvén wave and that the Lorentz force self-consistently acts to satisfy the current continuity. We also note that the propagation speed of the parallel vorticity is much slower than the

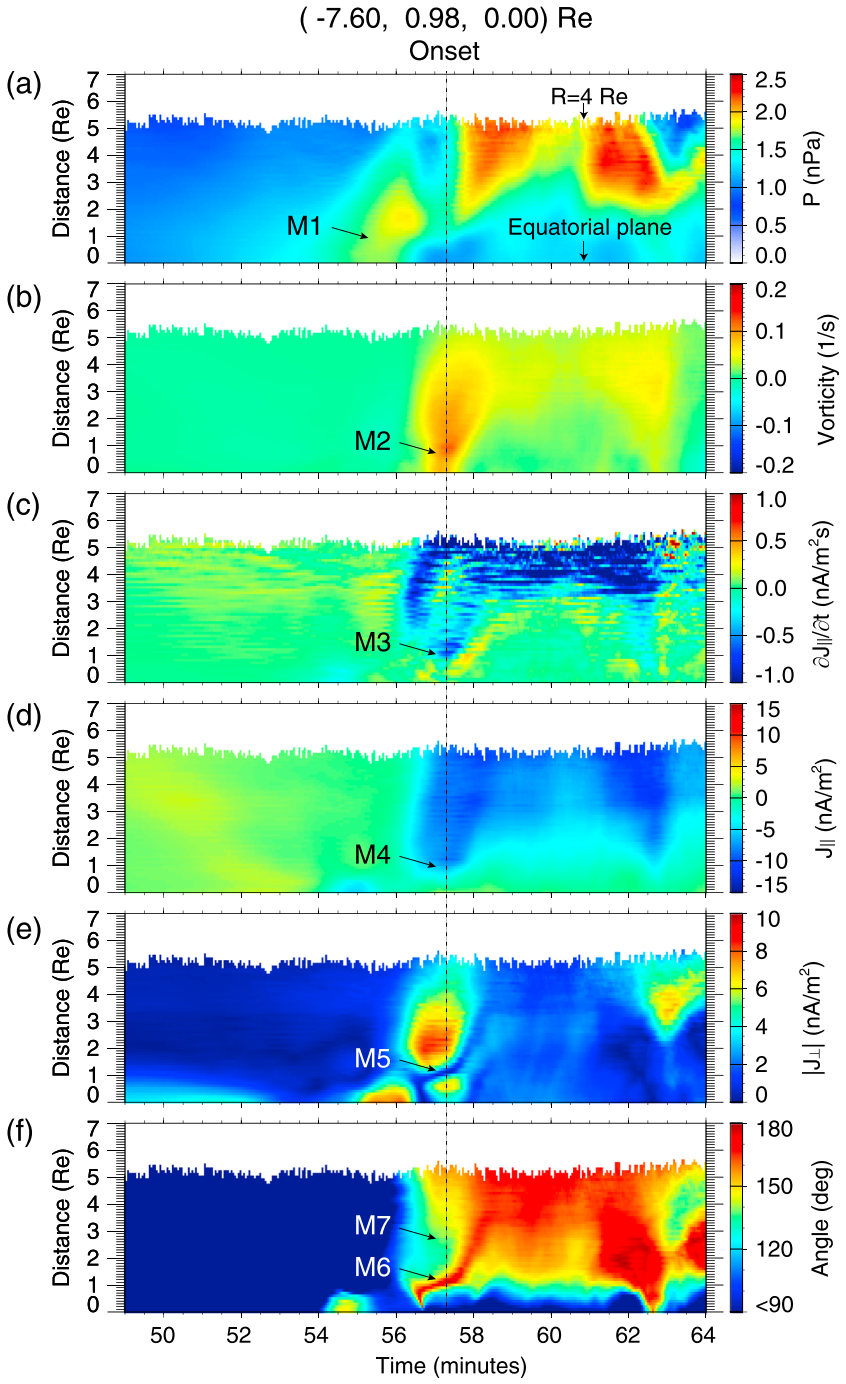

Figure 7. (a) Pressure, (b) parallel vorticity $\Omega_{||}$, (c) $\partial J_{||}/\partial t$, (d) field-aligned current $J_{||}$, (e) magnitude of the perpendicular current, and (f) angle between **J** and **B** as a function of time and distance along a magnetic field line passing through the westward edge of the incomplete current wedge at onset (t = 57.34 min). In each panel, the lowest distance corresponds to the equatorial plane, and the farthest distance corresponds to the geocentric distance of 4.0 Re.

local Alfvén speed. The propagation speed of the upward FAC region is close to that of the high-pressure region (Figure 8, M1).

Figure 9 summarizes snapshots of selected quantities in the Y–Z plane at $X = -4$ Re at onset. Figure 9a shows plasma pressure, which peaks at $Z \approx 2.5$ Re. The arrow indicates the perpendicular current density projected onto the Y–Z plane. The current flows anticlockwise in the Northern Hemisphere as if surrounding the high-

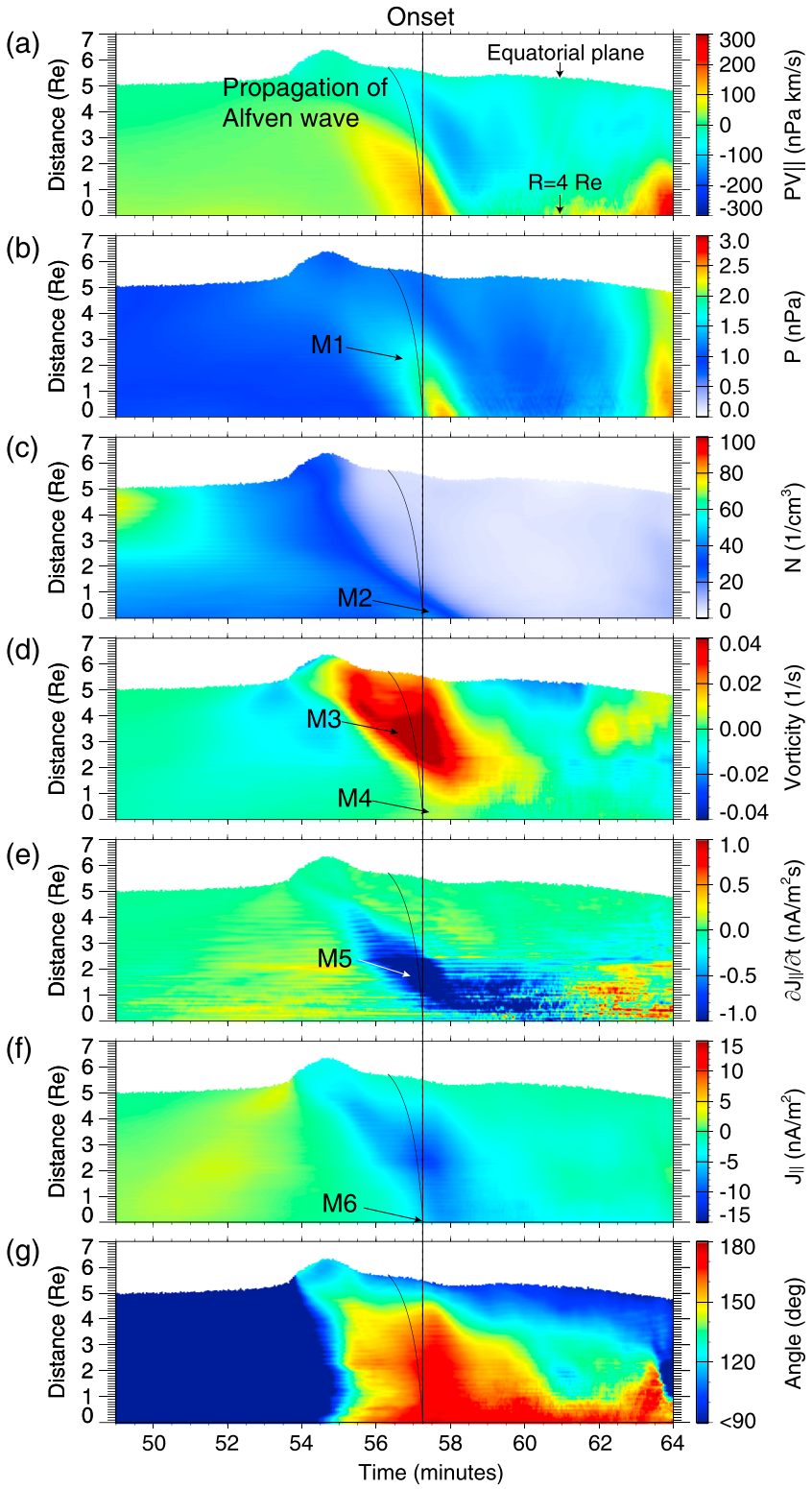

Figure 8. (a) $PV_{||}$, (b) pressure, (c) number density, (d) parallel vorticity $\Omega_{||}$, (e) $\partial J_{||}/\partial t$, (f) field-aligned current $J_{||}$, and (g) angle between **J** and **B** as a function of time and distance along a field line extending from the initial brightening taking place at onset (66.7 MLAT, 2318 MLT, t = 57.34 min). In each panel, the lowest distance corresponds to the geocentric distance of 4.0 Re, and the farthest distance corresponds to the equatorial plane. A black curve indicates the propagation of Alfvén wave calculated from the local Alfvén speed.

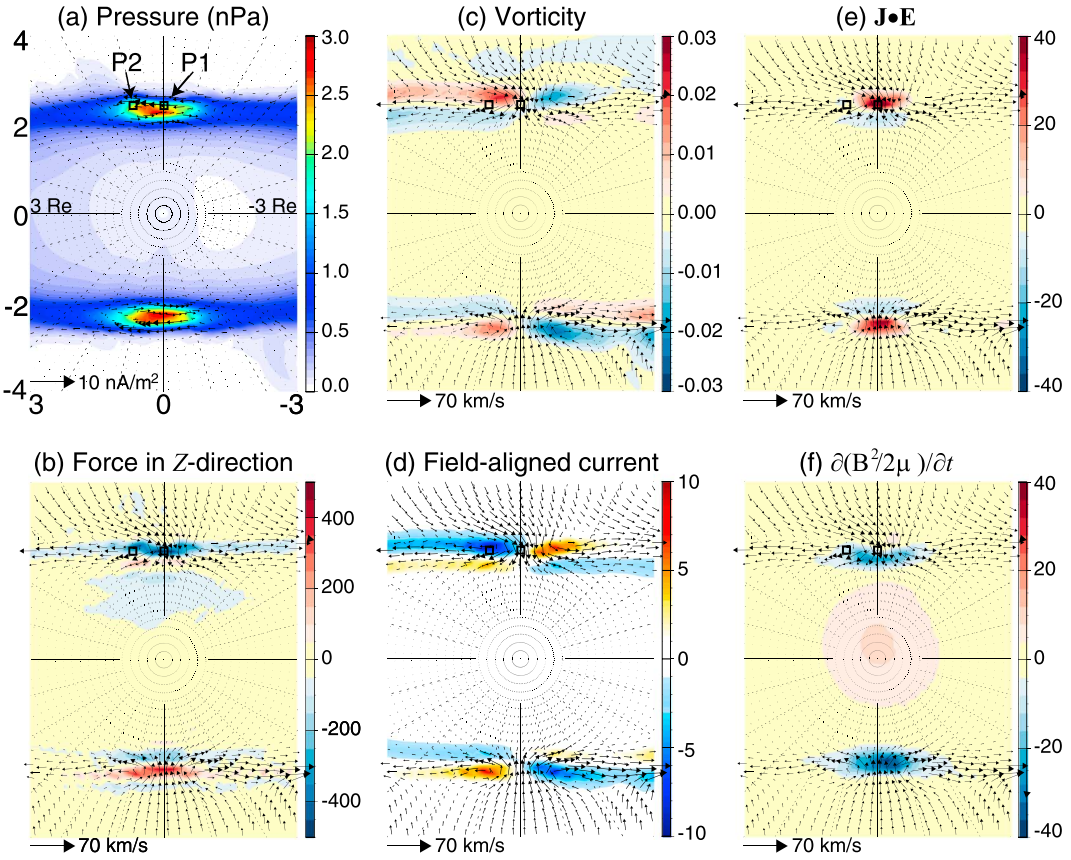

Figure 9. (a) Plasma pressure in nPa, (b) force density in the Z direction in 10^{-18} N/m^3, (c) vorticity of plasma flow in s^{-1}, (d) field-aligned current in nA/m^2 (negative value means upward current), (e) **J•E** in 10^{-12} W/m^3, and (f) $\partial(B^2/2\mu_0)/\partial t$ in 10^{-12} W/m^3 in the Y–Z plane at $X = -4$ Re at onset ($t = 57.34$ min). Dusk is to the left. An arrow in Figure 9a indicates the current density in the Y–Z plane. An arrow in Figures 9b–9f indicates the perpendicular velocity of plasma in the Y–Z plane. Two points, P_1 and P_2, are indicated by solid squares.

pressure region. Thus, this current appears to be the diamagnetic current. In Figure 9b, the Z component of the inertial force is shown. In an ideal MHD, the force density is given by

$$\begin{aligned} \mathbf{F}_i &= \mathbf{F}_T + \mathbf{F}_B + \mathbf{F}_P, \\ \mathbf{F}_i &= \rho \frac{d\mathbf{V}}{dt}, \\ \mathbf{F}_T &= \frac{1}{\mu_0}(\mathbf{B}\cdot\nabla)\mathbf{B} \\ \mathbf{F}_B &= -\nabla\left(\frac{B^2}{2\mu_0}\right), \\ \mathbf{F}_P &= -\nabla P, \end{aligned} \tag{4}$$

where $\mathbf{F}_i$, $\mathbf{F}_T$, $\mathbf{F}_B$, and $\mathbf{F}_P$ are the inertial force, the tension force, the magnetic pressure force, and the plasma pressure force, respectively; P is the plasma pressure; and ρ is the mass density of the plasma. In the Northern Hemisphere, the inertial force is directed toward the equatorial plane (negative value in Z) in the center of the high-pressure region. The arrow indicates perpendicular flow velocity $\mathbf{V}_\perp$ in the Y–Z plane. Because of the negative inertial force, plasma is accelerated toward the equatorial plane in the Northern Hemisphere. The plasma is then deflected away from the high-pressure region. Because of the deflection of the plasma flow, strong flow vorticity (shear) develops near the high-pressure region. Figure 9c shows the parallel vorticity $\Omega_{||}$. The vorticity shows a quadrupole structure in terms of its polarity. Figure 9d shows FACs. A negative value means the current flows antiparallel to the magnetic field, representing an upward FAC in the Northern Hemisphere. The polarity of the FACs also displays a quadrupole structure. The outer pair of the

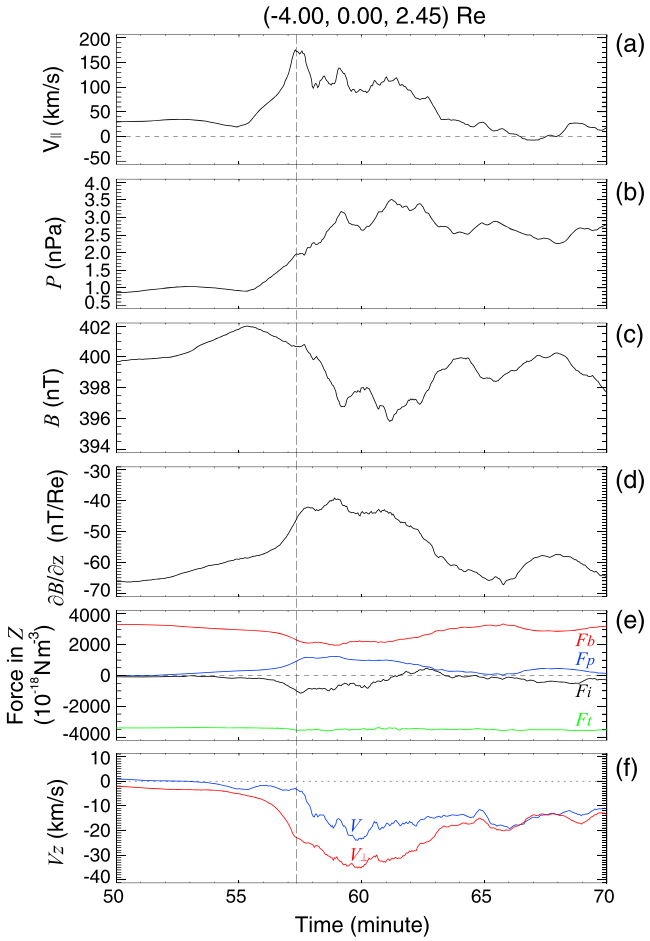

Figure 10. (a) Parallel flow velocity (positive parallel to the magnetic field), (b) plasma pressure, (c) magnitude of magnetic field, (d) gradient of the magnitude of magnetic field in the Z direction, (e) the force density in the Z direction, and (f) Z component of the plasma velocity at P_1, that is, (−4.00, 0.00, 2.45) Re. In Figure 10e, black, red, blue, and green lines indicate the inertial force, the magnetic pressure force, the plasma pressure force, and the tension force, respectively. In Figure 10f, blue and red lines indicate the velocity and the perpendicular velocity, respectively.

FACs is consistent with a Region 1-sense current (current flowing into the ionosphere on the dawnside and away from the ionosphere on the duskside). The inner pair is consistent with a Region 2-sense current (the direction of the FAC is opposite to that of the Region 1 current). An upward FAC is found where $\Omega_{||} > 0$ and vice versa. The two components of the energy transfer rate, that is, the two terms on the right-hand side of equation (3), are shown in Figures 9e and 9f. Negative values imply a source of electromagnetic energy, that is, a dynamo. The term $\partial(B^2/2\mu_0)/\partial t$ seems to act as a dynamo in the region where the Region 1-sense FAC flows. A similar flow pattern is shown in *Birn and Hesse* [2005, Figure 9], and a similar FAC pattern is also shown in *Birn et al.* [2004, Figure 17] and *Birn and Hesse* [2013, Figure 4].

In order to investigate the generation of the vorticity and the FAC, we focused on the two points P_1 (−4.00, 0.00, 2.45) Re and P_2 (−4.00, 0.70, 2.45) Re, indicated by solid squares in Figure 9. Point P_1 was selected to investigate the generation of the vorticity, and point P_2 to investigate the generation of the FAC. Figure 10 summarizes the time history of relevant quantities measured at P_1, at which the plasma is accelerated toward the equatorial plane. Major characteristics can be summarized as follows: (a) parallel velocity $V_{||}$ is maximized near the onset; (b) plasma pressure is increased because plasma is transported primarily by parallel flow; (c) the magnitude of the magnetic field, on the other hand, decreases. The anticorrelation between plasma pressure and the magnitude of the magnetic field implies that the magnetic field is decreased by the diamagnetic current (diamagnetic effect); (d) the gradient of the magnetic field in the Z direction increases (relaxes) because of the reduction of the magnetic field; (e) the tension force (green line) remains almost unchanged throughout the period of interest. The plasma pressure force (blue line) increases near onset in association with the increase in plasma pressure. The magnetic pressure force (red line) decreases (relaxes) in association with the decrease in the magnetic field. The decrease in the magnetic pressure force overcomes the increase in the plasma pressure force. The inertial force, which is a sum of $\mathbf{F}_T$, $\mathbf{F}_B$, and $\mathbf{F}_P$, is nonzero and is directed toward the equatorial plane (negative inertial force); (f) the negative inertial force accelerates the plasma in the negative Z direction (toward the equatorial plane).

Figure 11a summarizes plasma pressure, magnitude of the magnetic field, the Z component of the force density, and the Z component of the perpendicular plasma flow velocity as a function of Z at $X = -4.00$ Re and $Y = 0.00$ at onset. The dashed lines indicate parameters measured 137 s before the onset. At onset, the plasma pressure suddenly increases around $Z = 2.35$ Re (Figure 11, M1) because of earthward flow along a field line (Figure 4, M7). The magnitude of the magnetic field $|B|$ is decreased by the diamagnetic

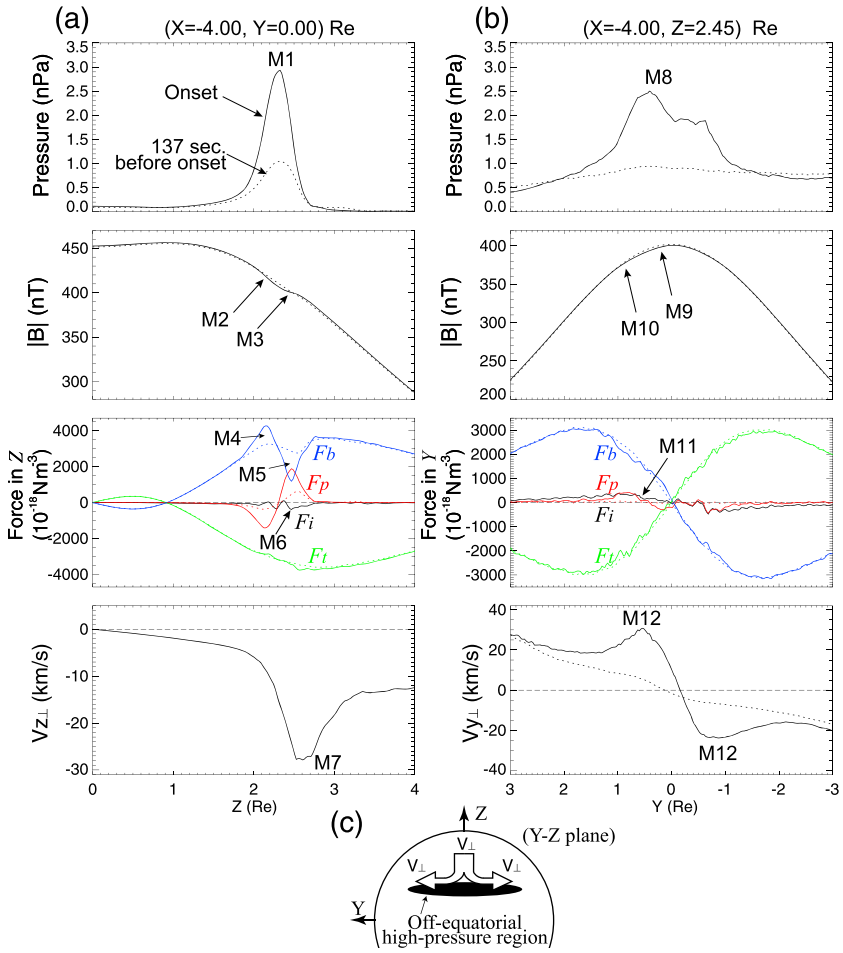

Figure 11. (a) Plasma pressure, magnitude of magnetic field, Z component of the force, and Z component of the perpendicular plasma flow as a function of Z at $X = -4$ Re and $Y = 0$ at onset, and (b) plasma pressure, magnitude of magnetic field, Y component of the force, and Y component of the perpendicular plasma flow as a function of Y at $X = -4$ Re and $Z = 2.45$ Re at onset ($t = 57.34$ min). In Figure 11c, a schematic drawing of the direction of the plasma flow in the Y–Z plane at $X = -4$ Re is present.

current. Because the magnitude of the background magnetic field decreases with Z at $Z > 1$ Re, the formation of the small dip in $|B|$ results in a steeper slope at lower Z (Figure 11, M2) and a shallow slope at higher Z (Figure 11, M3). The steep slope in $|B|$ results in an increase in the magnetic pressure force (Figure 11, M4), while the shallow slope results in a decrease in the magnetic pressure force (Figure 11, M5) that overcomes the increase in plasma pressure. Consequently, a negative inertial force appears (Figure 11, M6), which accelerates plasma from the high-$|Z|$ region toward the center of the high-pressure region (Figure 11, M7).

Almost the same situation exists for the Y direction. Figure 11b summarizes plasma pressure, magnitude of the magnetic field, the Y component of the force density, and the Y component of the perpendicular plasma flow as a function of Y at $X = -4.00$ Re and $Z = 2.45$ Re at onset. The plasma pressure rapidly increases near midnight (Figure 11, M8), while $|B|$ is slightly decreased by the diamagnetic effect. Because the magnitude of the background magnetic field peaks near midnight, a local decrease in $|B|$ results in a steeper slope near midnight (Figure 11, M9) and a shallow slope away from midnight (Figure 11, M10). The steep slope of $|B|$ near midnight results in a magnetic pressure force increase that overcomes the plasma pressure force. A positive (negative) inertial force is found on the duskside (dawnside) (Figure 11, M11), and the plasma is accelerated away from midnight (Figure 11, M12).

Figure 11c shows a schematic drawing of the flow direction in the Y–Z plane. A force balance (among $\mathbf{F}_T$, $\mathbf{F}_B$, and $\mathbf{F}_P$) against the sudden increase in the plasma pressure force is not quickly achieved in the MHD. Almost the

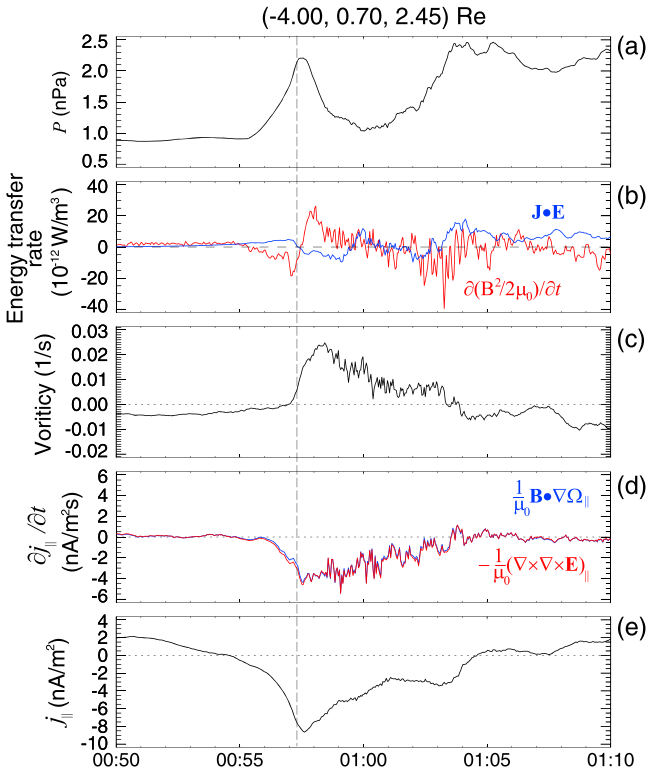

Figure 12. (a) Plasma pressure, (b) energy transfer rate [red color for $\partial(B^2/2\mu_0)/\partial t$ and blue color for **J•E**], (c) vorticity of the plasma flow parallel to the magnetic field, (d) $\partial J_{||}/\partial t$, and (e) the field-aligned current (negative upward) at P_2, that is, (−4.00, 0.80, 2.45) Re.

same situation is found in the near-Earth plasma sheet just after the expansion onset, when plasma pressure suddenly increases [*Ebihara and Tanaka*, 2013]. Because of the force imbalance, plasma is pulled into the off-equatorial high-pressure region from high latitude and is discharged away from it. The pulling and discharging of the plasma generate flow vortices. A positive vorticity is found in the western section of the upper part of the plasma bullet, while a negative vorticity occurs in the eastern section (Figure 9c).

Next, we address the question regarding the generation of FAC and dynamo. Figure 12 shows the temporal variation of selected quantities measured at P_2, which is located the western section of the upper part of the off-equatorial high-pressure region. Major characteristics can be summarized as follows: (a) plasma pressure peaks near the onset. As the off-equatorial high-pressure region propagates earthward along a field line, plasma pressure shows a positive excursion when observed at a fixed point; (b) at and just before the onset, **J•E** is slightly positive, whereas $\partial(B^2/2\mu_0)/\partial t$ is negative. The opposite tendency is found after the onset. Both terms appear to be responsible for the generation of electromagnetic energy at this point. The magnitude of the magnetic field $|B|$ is decreased by the diamagnetic current in the high-pressure region. When observed at a fixed point, $|B|$ shows a negative excursion as the high-pressure region propagates earthward along a field line. Thus, $\partial(B^2/2\mu_0)/\partial t$ shows a bipolar variation; (c) vorticity rapidly increases near the onset because of pull-in and discharge of ambient plasma; (d) the red line indicates the time derivative of FAC given by equation (1), and the blue line indicates that given by equation (2). Both values are almost identical, suggesting that the upward FAC is generated by parallel vorticity; (e) the upward FAC is intensified near the onset. The integral of $\partial J_{||}/\partial t$ with respect to time is not equal to $J_{||}$ as is pointed out above.

Figure 13 shows the energy transfer rate in the meridional plane at 2300 MLT. At onset, strong dynamo regions (**J•E** < 0) appear in the near-Earth region (<8 Re), which we call near-Earth dynamo. The region where $\partial(B^2/2\mu_0)/\partial t < 0$ is found at low altitude (Figure 13, M1). This dynamo is related to the reduction of the local magnetic field due to the diamagnetic current. The dynamo region is also found near the equatorial plane (Figure 13, M2), which can also be seen in Figure 5. This dynamo is associated with the eastward diamagnetic current. Both dynamo regions, together with the high-latitude mantle region, may be involved in supplying electromagnetic energy to the ionosphere at the onset.

4. Discussion

The formation of the off-equatorial high-pressure region may be a natural consequence of flow braking of the earthward fast flow (or bursty bulk flow). Earthward fast flows are frequently observed in the tail, but a one-to-one correspondence between an earthward fast flow and a substorm has been questionable [*Angelopoulos et al.*, 1994]. *Juusola et al.* [2011] conducted a statistical analysis of earthward fast flows and found that an earthward fast flow may occur regardless of the substorm phase (quiet, growth, expansion, and recovery) and that the occurrence frequency of medium- and high-speed flows (>100 km s^{-1}) increases

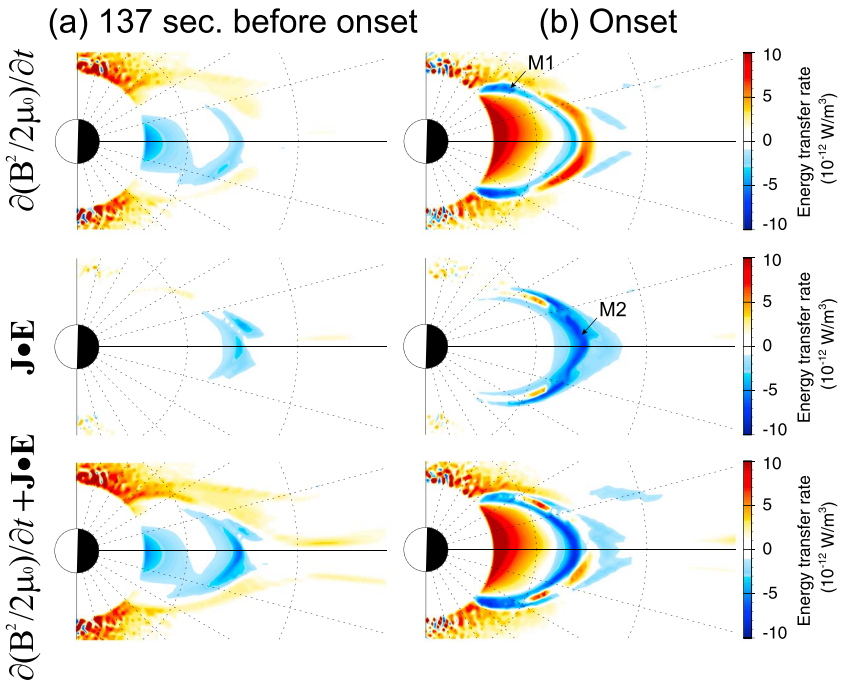

Figure 13. Energy transfer rate due to (top) $\partial(B^2/2\mu_0)/\partial t$, (middle) **J•E**, and (bottom) sum of them in the meridional plane at 23 MLT (left) 137 s before the onset and (right) at onset. Sun is to the left. The inner and outer circles indicate the radial distance of 5 Re and 10 Re, respectively.

during the expansion phase. These observations suggest that off-equatorial high-pressure regions are generated regardless of the substorm phase. The location where flow braking takes place is primarily determined by competition between the tailward pressure force and the earthward tension force. It is speculated that after a prolonged quiet time, flow braking takes place in the inner region because the tailward plasma pressure force is weak. After a substorm (earthward fast flow) occurs, the plasma pressure in the inner magnetosphere would remain strong. If another fast flow occurred soon after the first one, flow braking would take place in the outer region and hence the off-equatorial high-pressure region would reach higher latitude because of the strong tailward plasma pressure force. These processes may be related to the occurrence of auroral streamers that are found during the expansion and recovery phases [e.g., *Nakamura et al.*, 1993, 2001; *Henderson et al.*, 1998; *Sergeev et al.*, 1999, 2000, 2004; *Zesta et al.*, 2000, 2002, 2006; *Kauristie et al.*, 2000; *Shi et al.*, 2012].

The off-equatorial high-pressure region may also contribute to the short-lived intensification of the aurora observed during a pseudobreakup event [e.g., *Nakamura et al.*, 1994; *Partamies et al.*, 2003; *Yago et al.*, 2007] or before the beginning of substorm expansion [e.g., *Saito et al.*, 2010]. Pseudobreakups are accompanied by particle injection and dipolarization [*Koskinen et al.*, 1993; *Nakamura et al.*, 1994]. The differences between pseudobreakups and full breakups are the degree of ionospheric conductivity [*Kan et al.*, 1988], strength and temporal evolution [*Koskinen et al.*, 1993], intensity, and scale size of the magnetospheric source [*Nakamura et al.*, 1994]. We will discuss the difference between pseudobreakups and full breakups as well as the evolution of the auroral structures during the expansion phase in a separate manuscript.

Lui et al. [1977] observed high-speed, field-aligned, earthward bulk flows at -10 Re $> X > -30$ Re with an average duration time of ~12 min near the upper and lower boundaries of the plasma sheet. The authors suggested a possible connection to a discrete auroral region. *Baumjohann et al.* [1988] found that the occurrence rate of high-speed, field-aligned earthward bulk flows is higher during high AE. Such parallel flows are found in the plasma sheet boundary layer (PSBL) [e.g., *Eastman et al.*, 1984; *Miyashita et al.*, 2000]. Field-aligned, earthward bulk flows would result in the formation of an off-equatorial high-pressure region that generates FAC if they contribute to the pressure enhancement. If so, the off-equatorial high-pressure region generated near the PSBL may also result in an intensification of the upward FAC near the poleward edge of the auroral oval, like a poleward boundary intensification [e.g., *Lyons et al.*, 1999, 2012; *Zesta et al.*, 2002, 2006]. Further

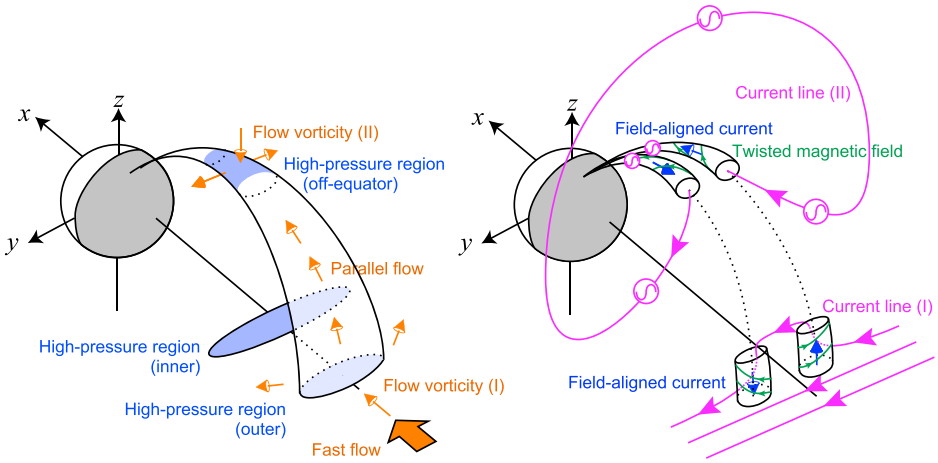

Figure 14. Schematic drawing of the possible mechanism for the initial brightening of aurora. The earthward fast flow generates flow vorticity (I) and field-aligned current near the equatorial plane. The cross-tail current, current line (I), is diverted from the equatorial plane but is not connected with the ionosphere because of the strong diamagnetic current. The off-equatorial high-pressure region appears at off-equator and propagates earthward along a field line. Flow vorticity (II) and field-aligned current are generated in the upper part of the off-equatorial high-pressure region. Current line (II), extending from the initial brightening, is connected with the mantle region by way of the near-Earth dynamo region associated with the high-pressure region (inner). The upward FAC generated in the off-equatorial high-pressure region is connected with the ionosphere, which may manifest the initial brightening. (Illustration based on Figure 19 in *Birn et al.* [2004].)

investigation is needed to confirm the relationship between these auroral structures and the off-equatorial high-pressure region.

The proposed mechanism is comprehensive. Some observations may have provided evidence for a part of the mechanisms. *Nakamura et al.* [2014] found a flow vortex in the *Y–Z* plane, far distant from the equatorial plane, in association with earthward flow bursts. The sense of the flow vortex is consistent with the upward FAC and may be consistent with our results as shown in Figure 9d. Our simulation results suggest that the initial brightening is associated with the formation of the outer pressure peak (Figure 5, M4), which retreats tailward [*Tanaka et al.*, 2010, Figure 12]. The tailward retreat of the outer pressure peak was recently identified by the THEMIS satellites [*Yao et al.*, 2015]. Comprehensive observations that use optical auroral and satellite measurements in the near-Earth tail at equator and off-equator are needed to confirm the existence of the proposed mechanism.

5. Conclusions

We have investigated the generation of a Region 1-sense FAC that may manifest the initial brightening at the beginning of the expansion phase of a substorm. A suggested mechanism is shown schematically in Figure 14 and can be summarized as follows.

1. Formation of a near-Earth neutral line causes the development of an earthward tension force and results in two high-pressure regions near the equatorial plane. The inner region is formed by plasma squeezing [*Haerendel*, 2010; *Tanaka et al.*, 2010], while the outer region is formed by flow braking [*Birn et al.*, 2004; *Tanaka et al.*, 2010].
2. The earthward (perpendicular) flow is deflected toward dawn and dusk, and two flow vortices are formed near the equatorial plane. These flow vortices generate the Region 1-sense FAC. The FAC diverts the dawn-dusk cross-tail current from the equatorial plane. The shape of the current line is similar to the current wedge, but the leg of the current wedge is too short to reach the ionosphere. The current line is easily deflected by the strong diamagnetic current (perpendicular current) so that the current line is not necessarily connected with the ionosphere.
3. Flow braking (the convergence of the flow) gives rise to a pressure gradient along a field line. Plasma is accelerated toward the Earth. Plasma pressure increases in an off-equatorial region, and the high-pressure region propagates toward Earth along a field line. We call this an off-equatorial high-pressure region.

4. The off-equatorial high-pressure region pulls ambient plasma from high latitudes toward the center of the off-equatorial high-pressure region and discharges it away from its center, generating *vorticity at off-equator*. This vorticity builds up the Region 1-sense FAC in the upper part of the off-equatorial high-pressure region, and the Region 2-sense FAC in its lower part.
5. When the upward FAC generated near the off-equatorial high-pressure region is connected with the ionosphere, the initial brightening starts in the ionosphere.

There are at least three regions that generate electromagnetic energy along the current line extending from the initial brightening, just above the equatorial plane in the inner magnetosphere ($\mathbf{J}\cdot\mathbf{E} < 0$, Dynamo I), the high-latitude mantle region ($\mathbf{J}\cdot\mathbf{E} < 0$, Dynamo II), and the low-altitude region [$\partial(B^2/2\mu_0)/\partial t < 0$, Dynamo III]. As Dynamo (II) steadily exists under the southward IMF [*Tanaka*, 2007], Dynamo (I) and Dynamo (III) would be most important for the initial brightening. Dynamo (I) is associated with the inner high-pressure region, while the Region 1-sense FAC around the off-equatorial high-pressure region is associated with the outer high-pressure region. Thus, formation of the two-layered high-pressure regions (Figure 4, M3 and M5) may play an important role in the initial brightening. It is suggested that the upward FAC manifesting the initial brightening must be generated in the near-Earth region where the magnetic field is strong and the diamagnetic current is relatively small in comparison with the FAC.

Acknowledgments
We thank Takashi Kikuchi, Takeshi Sakanoi, Akimasa Ieda, and Kazuo Shiokawa for fruitful comments and discussion. The computer simulation was performed on the KDK computer system at Research Institute for Sustainable Humanosphere (RISH), Kyoto University. This study was supported by KAKENHI, Grant-in-Aid for Scientific Research (B) 24340119 and 15H03732. The simulation data are available upon request.

Michael Liemohn thanks the reviewers for their assistance in evaluating the paper.

References

Aikio, A. T., T. Lakkala, A. Kozlovsky, and P. J. S. Williams (2002). Electric fields and currents of stable drifting auroral arcs in the evening sector, *J. Geophys. Res.*, *107*(A12), 1424, doi:10.1029/2001JA009172.

Akasofu, S.-I. (1964), The development of the auroral substorm, *Planet. Space Sci.*, *12*, 273–282.

Angelopoulos, V., C. F. Kennel, F. V. Coroniti, R. Pellat, M. G. Kivelson, R. J. Walker, C. T. Russell, W. Baumjohann, W. C. Feldman, and J. T. Gosling (1994), Statistical characteristics of bursty bulk flow events, *J. Geophys. Res.*, *99*(A11), 21,257–21,280, doi:10.1029/94JA01263.

Angelopoulos, V., et al. (2008), Tail reconnection triggering substorm onset, *Science*, *321*, 931, doi:10.1126/science.1160495.

Baumjohann, W., G. Paschmann, N. Sckopke, C. A. Cattell, and C. W. Carlson (1988), Average ion moments in the plasma sheet boundary layer, *J. Geophys. Res.*, *93*(A10), 11,507–11,520, doi:10.1029/JA093iA10p11507.

Birn, J., and M. Hesse (2005), Energy release and conversion by reconnection in the magnetotail, *Ann. Geophys.*, *23*, 3365–3373, doi:10.5194/angeo-23-3365-2005.

Birn, J., and M. Hesse (2013), The substorm current wedge in MHD simulations, *J. Geophys. Res. Space Physics*, *118*, 3364–3376, doi:10.1002/jgra.50187.

Birn, J., M. Hesse, G. Haerendel, W. Baumjohann, and K. Shiokawa (1999), Flow braking and the substorm current wedge, *J. Geophys. Res.*, *104*(A9), 19,895–19,903, doi:10.1029/1999JA900173.

Birn, J. M., J. Raeder, Y. L. Wang, R. A. Wolf, and M. Hesse (2004), On the propagation of bubbles in the magnetotail, *Ann. Geophys.*, *22*, 1773–1786.

Chen, C. X., and R. A. Wolf (1999), Theory of thin-filament motion in Earth's magnetotail and its application to bursty bulk flows, *J. Geophys. Res.*, *104*(A7), 14,613–14,626, doi:10.1029/1999JA900005.

Cheng, C. Z., and A. T. Y. Lui (1998), Kinetic ballooning instability for substorm onset and current disruption observed by AMPTE/CCE, *Geophys. Res. Lett.*, *25*(21), 4091–4094, doi:10.1029/1998GL900093.

Craven, J. D., L. A. Frank, and S.-I. Akasofu (1989), Propagation of a westward traveling surge and the development of persistent auroral features, *J. Geophys. Res.*, *94*(A6), 6961–6967, doi:10.1029/JA094iA06p06961.

de la Beaujardiere, O., R. Vondrak, and M. Baron (1977), Radar observations of electric fields and currents associated with auroral arcs, *J. Geophys. Res.*, *82*(32), 5051–5062, doi:10.1029/JA082i032p05051.

Deehr, C., and D. Lummerzheim (2001), Ground-based optical observations of hydrogen emission in the auroral substorm, *J. Geophys. Res.*, *106*(A1), 33–44, doi:10.1029/2000JA002010.

Eastman, T. E., L. A. Frank, W. K. Peterson, and W. Lennartsson (1984), The plasma sheet boundary layer, *J. Geophys. Res.*, *89*(A3), 1553–1572, doi:10.1029/JA089iA03p01553.

Ebihara, Y., and T. Tanaka (2013), Fundamental properties of substorm time energetic electrons in the inner magnetosphere, *J. Geophys. Res. Space Physics*, *118*, 1589–1603, doi:10.1002/jgra.50115.

Ebihara, Y., T. Tanaka, and T. Kikuchi (2014), Counter equatorial electrojet and overshielding after substorm onset: Global MHD simulation study, *J. Geophys. Res. Space Physics*, *119*, 7281–7296, doi:10.1002/2014JA020065.

Elphinstone, R. D., et al. (1995), Observations in the vicinity of substorm onset: Implications for the substorm process, *J. Geophys. Res.*, *100*(A5), 7937–7969, doi:10.1029/94JA02938.

Fukuda, Y., M. Hirahara, K. Asamura, T. Sakanoi, Y. Miyoshi, T. Takada, A. Yamazaki, K. Seki, and Y. Ebihara (2014), Electron properties in inverted-V structures and their vicinities based on Reimei observations, *J. Geophys. Res. Space Physics*, *119*, 3650–3663, doi:10.1002/2013JA018938.

Haerendel, G. (2010), Equatorward moving arcs and substorm onset, *J. Geophys. Res.*, *115*, A07212, doi:10.1029/2009JA015117.

Hasegawa, A., and T. Sato (1979), Generation of field aligned current during substorm, in *Dynamics of the Magnetosphere*, edited by S.-I. Akasofu, pp. 529–542, D. Reidel, Norwell, Mass.

Henderson, M. G., G. D. Reeves, and J. S. Murphree (1998), Are north–south structures an ionospheric manifestation of bursty bulk flows?, *Geophys. Res. Lett.*, *25*(19), 3737, doi:10.1029/98GL02692.

Heppner, J. P. (1972), The Harang discontinuity in auroral belt ionospheric currents, *Geophys. Norv.*, *29*, 105–120.

Iijima, T., and T. A. Potemra (1976), The amplitude distribution of field-aligned currents at northern high latitudes observed by Triad, *J. Geophys. Res.*, *81*(13), 2165–2174, doi:10.1029/JA081i013p02165.

Juusola, L., N. Østgaard, E. Tanskanen, N. Partamies, and K. Snekvik (2011), Earthward plasma sheet flows during substorm phases, *J. Geophys. Res.*, *116*, A10228, doi:10.1029/2011JA016852.

Kadokura, A., A.-S. Yukimatu, M. Ejiri, T. Oguti, M. Pinnock, and M. R. Hairston (2002), Detailed analysis of a substorm event on 6 and 7 June 1989, 1, Growth phase evolution of nightside auroral activities and ionospheric convection toward expansion phase onset, *J. Geophys. Res.*, *107*(A12), 1479, doi:10.1029/2001JA009127.

Kamide, Y., W. Sun, and S.-I. Akasofu (1996), The average ionospheric electrodynamics for the different substorm phases, *J. Geophys. Res.*, *101*(A1), 99–109, doi:10.1029/95JA02990.

Kan, J. R., L. Zhu, and S.-I. Akasofu (1988), A theory of substorms: Onset and subsidence, *J. Geophys. Res.*, *93*(A6), 5624–5640, doi:10.1029/JA093iA06p05624.

Kauristie, K., V. A. Sergeev, M. Kubyshkina, T. I. Pulkkinen, V. Angelopoulos, T. Phan, R. P. Lin, and J. A. Slavin (2000), Ionospheric current signatures of transient plasma sheet flows, *J. Geophys. Res.*, *105*(A5), 10,677–10,690, doi:10.1029/1999JA900487.

Keiling, A., et al. (2009), Substorm current wedge driven by plasma flow vortices: THEMIS observations, *J. Geophys. Res.*, *114*, A00C22, doi:10.1029/2009JA014114.

Kepko, L., R. L. McPherron, O. Amm, S. Apatenkov, W. Baumjohann, J. Birn, M. Lester, R. Nakamura, T. I. Pulkkinen, and V. Sergeev (2014), Substorm current wedge revisited, *Space Sci. Rev.*, *190*, 1–46, doi:10.1007/s11214-014-0124-9.

Koskinen, H. E. J., R. E. Lopez, R. J. Pellinen, T. I. Pulkkinen, D. N. Baker, and T. Bösinger (1993), Pseudobreakup and substorm growth phase in the ionosphere and magnetosphere, *J. Geophys. Res.*, *98*(A4), 5801–5813, doi:10.1029/92JA02482.

Liou, K., P. T. Newell, D. G. Sibeck, C.-I. Meng, M. Brittnacher, and G. Parks (2001), Observation of IMF and seasonal effects in the location of auroral substorm onset, *J. Geophys. Res.*, *106*(A4), 5799–5810, doi:10.1029/2000JA003001.

Lopez, R. E., and A. T. Y. Lui (1990), A multisatellite case study of the expansion of a substorm current wedge in the near-Earth magnetotail, *J. Geophys. Res.*, *95*(A6), 8009–8017, doi:10.1029/JA095iA06p08009.

Lui, A. T. Y. (1996), Current disruption in the Earth's magnetosphere: Observations and models, *J. Geophys. Res.*, *101*(A6), 13,067–13,088, doi:10.1029/96JA00079.

Lui, A. T. Y., and J. R. Burrows (1978), On the location of auroral arcs near substorm onsets, *J. Geophys. Res.*, *83*(A7), 3342–3348, doi:10.1029/JA083iA07p03342.

Lui, A. T. Y., E. W. Hones Jr., F. Yasuhara, S.-I. Akasofu, and S. J. Bame (1977), Magnetotail plasma flow during plasma sheet expansions: VELA 5 and 6 and IMP 6 observations, *J. Geophys. Res.*, *82*(7), 1235–1243, doi:10.1029/JA082i007p01235.

Lui, A. T. Y., A. Mankofsky, C.-L. Chang, K. Papadopoulos, and C. S. Wu (1990), A current disruption mechanism in the neutral sheet: A possible trigger for substorm expansions, *Geophys. Res. Lett.*, *17*(6), 745–748, doi:10.1029/GL017i006p00745.

Lyatsky, W., L. L. Cogger, B. Jackel, A. M. Hamza, W. J. Hughes, D. Murr, and O. Rasmussen (2001), Substorm development as observed by Interball UV imager and 2-D magnetic array, *J. Atmos. Sol. Terr. Phys.*, *63*, 1609–1621, doi:10.1016/S1364-6826(01)00045-1.

Lyons, L. R., T. Nagai, G. T. Blanchard, J. C. Samson, T. Yamamoto, T. Mukai, A. Nishida, and S. Kokubun (1999), Association between Geotail plasma flows and auroral poleward boundary intensifications observed by CANOPUS photometers, *J. Geophys. Res.*, *104*(A3), 4485–4500, doi:10.1029/1998JA900140.

Lyons, L. R., Y. Nishimura, X. Xing, A. Runov, V. Angelopoulos, E. Donovan, and T. Kikuchi (2012), Coupling of dipolarization front flow bursts to substorm expansion phase phenomena within the magnetosphere and ionosphere, *J. Geophys. Res.*, *117*, A02212, doi:10.1029/2011JA017265.

Marghitu, O., T. Karlsson, B. Klecker, G. Haerendel, and J. McFadden (2009), Auroral arc and oval electrodynamics in the Harang region, *J. Geophys. Res.*, *114*, A03214, doi:10.1029/2008JA013630.

Marklund, G., I. Sandahl, and H. Opgenoorth (1982), A study of the dynamics of a discrete auroral arc, *Planet. Space Sci.*, *30*, 179–197.

McPherron, R. L., C. T. Russell, and M. P. Aubry (1973), Satellite studies of magnetospheric substorms on August 15, 1968: 9. Phenomenological model for substorms, *J. Geophys. Res.*, *78*(16), 3131–3149, doi:10.1029/JA078i016p03131.

Mende, S. B., C. W. Carlson, H. U. Frey, L. M. Peticolas, and N. Østgaard (2003), FAST and IMAGE-FUV observations of a substorm onset, *J. Geophys. Res.*, *108*(A9), 1344, doi:10.1029/2002JA009787.

Miyashita, Y., S. Machida, T. Mukai, Y. Saito, K. Tsuruda, H. Hayakawa, and P. R. Sutcliffe (2000), A statistical study of variations in the near and middistant magnetotail associated with substorm onsets: GEOTAIL observations, *J. Geophys. Res.*, *105*(A7), 15,913–15,930, doi:10.1029/1999JA000392.

Moriguchi, T., A. Nakamizo, T. Tanaka, T. Obara, and H. Shimazu (2008), Current systems in the Jovian magnetosphere, *J. Geophys. Res.*, *113*, A05204, doi:10.1029/2007JA012751.

Nagai, T. (1982), Observed magnetic substorm signatures at synchronous altitude, *J. Geophys. Res.*, *87*(A6), 4405–4417, doi:10.1029/JA087iA06p04405.

Nagai, T., M. Fujimoto, Y. Saito, S. Machida, T. Terasawa, R. Nakamura, T. Yamamoto, T. Mukai, A. Nishida, and S. Kokubun (1998), Structure and dynamics of magnetic reconnection for substorm onsets with Geotail observations, *J. Geophys. Res.*, *103*(A3), 4419–4440, doi:10.1029/97JA02190.

Nakamura, R., T. Oguti, T. Yamamoto, and S. Kokubun (1993), Equatorward and poleward expansion of the auroras during auroral substorm, *J. Geophys. Res.*, *98*(A4), 5743–5759, doi:10.1029/92JA02230.

Nakamura, R., D. N. Baker, T. Yamamoto, R. D. Belian, E. A. Bering III, J. R. Benbrook, and J. R. Theall (1994), Particle and field signatures during pseudobreakup and major expansion onset, *J. Geophys. Res.*, *99*(A1), 207–221, doi:10.1029/93JA02207.

Nakamura, R., W. Baumjohann, R. Schödel, M. Brittnacher, V. A. Sergeev, M. Kubyshkina, T. Mukai, and K. Liou (2001), Earthward flow bursts, auroral streamers, and small expansions, *J. Geophys. Res.*, *106*(A6), 10,791–10,802, doi:10.1029/2000JA000306.

Nakamura, R., et al. (2014), Low-altitude electron acceleration due to multiple flow bursts in the magnetotail, *Geophys. Res. Lett.*, *41*, 777–784, doi:10.1002/2013GL058982.

Nielsen, E., and R. A. Greenwald (1979), Electron flow and visual aurora at the Harang discontinuity, *J. Geophys. Res.*, *84*(A8), 4189–4199, doi:10.1029/JA084iA08p04189.

Nishida, A., and N. Nagayama (1973), Synoptic survey for the neutral line in the magnetotail during the substorm expansion phase, *J. Geophys. Res.*, *78*(19), 3782–3798, doi:10.1029/JA078i019p03782.

Ohtani, S. (1998), Earthward expansion of tail current disruption: Dual-satellite study, *J. Geophys. Res.*, *103*(A4), 6815–6825, doi:10.1029/98JA00013.

Partamies, N., O. Amm, K. Kauristie, T. I. Pulkkinen, and E. Tanskanen (2003), A pseudo-breakup observation: Localized current wedge across the postmidnight auroral oval, *J. Geophys. Res.*, *108*(A1), 1020, doi:10.1029/2002JA009276.

Paschmann, G., S. Haaland, and R. Treumann (Eds.) (2002), *Auroral Plasma Physics*, Kluwer Acad., Boston, Mass.

Rostoker, G., A. Vallance Jones, R. L. Gattinger, C. D. Anger, and J. S. Murphree (1987), The development of the substorm expansive phase: The "eye" of the substorm, *Geophys. Res. Lett.*, *14*(4), 399–402, doi:10.1029/GL014i004p00399.

Saito, M. H., Y. Miyashita, M. Fujimoto, K. Liou, Y. Saito, and J. B. Sigwarth (2010), Stepwise feature of aurora during substorm expansion compared with the near-Earth tail dipolarization: Possible types of substorm dynamics, *J. Geophys. Res.*, *115*, A02207, doi:10.1029/2009JA014572.

Samson, J. C., L. R. Lyons, P. T. Newell, F. Creutzberg, and B. Xu (1992), Proton aurora and substorm intensifications, *Geophys. Res. Lett.*, *9*(21), 2167–2170, doi:10.1029/92GL02184.
Sato, T., and T. Iijima (1979), Primary sources of large-scale Birkeland currents, *Space Sci. Rev.*, *24*, 347–366.
Sergeev, V., et al. (2008), Study of near-Earth reconnection events with Cluster and Double Star, *J. Geophys. Res.*, *113*, A07S36, doi:10.1029/2007JA012902.
Sergeev, V. A., and A. G. Yahnin (1979), The features of auroral bulge expansion, *Planet. Space Sci.*, *27*, 1429–1440.
Sergeev, V. A., V. Angelopoulos, J. T. Gosling, C. A. Cattell, and C. T. Russell (1996), Detection of localized, plasma-depleted flux tubes or bubbles in the midtail plasma sheet, *J. Geophys. Res.*, *101*(A5), 10,817–10,826, doi:10.1029/96JA00460.
Sergeev, V. A., K. Liou, C.-I. Meng, P. T. Newell, M. Brittnacher, G. Parks, and G. D. Reeves (1999), Development of auroral streamers in association with impulsive injections to the inner magnetotail, *Geophys. Res. Lett.*, *26*(3), 417–420, doi:10.1029/1998GL900311.
Sergeev, V. A., et al. (2000), Multiple-spacecraft observation of a narrow transient plasma jet in the Earth's plasma sheet, *Geophys. Res. Lett.*, *27*(6), 851–854, doi:10.1029/1999GL010729.
Sergeev, V. A., K. Liou, P. T. Newell, S.-I. Ohtani, M. R. Hairston, and F. Rich (2004), Auroral streamers: Characteristics of associated precipitation, convection and field-aligned currents, *Ann. Geophys.*, *22*, 537–548.
Shi, Y., E. Zesta, L. R. Lyons, J. Yang, A. Boudouridis, Y. S. Ge, J. M. Ruohoniemi, and S. Mende (2012), Two-dimensional ionospheric flow pattern associated with auroral streamers, *J. Geophys. Res.*, *117*, A02208, doi:10.1029/2011JA017110.
Shiokawa, K., W. Baumjohann, and G. Haerendel (1997), Braking of high-speed flows in the near-Earth tail, *J. Geophys. Res.*, *24*(10), 1179–1082, doi:10.1029/97GL01062.
Shiokawa, K., G. Haerendel, and W. Baumjohann (1998), Azimuthal pressure gradient as driving force of substorm currents, *Geophys. Res. Lett.*, *25*(7), 959–962, doi:10.1029/98GL00540.
Song, Y., and R. L. Lysak (2001a), Towards a new paradigm: From a quasi-steady description to a dynamical description of the magnetosphere, *Space Sci. Rev.*, *95*, 273–292.
Song, Y., and R. L. Lysak (2001b), The physics in the auroral dynamo regions and auroral particle acceleration, *Phys. Chem. Earth*, *26*, 33.
Stenbaek-Nielsen, H. C., T. J. Hallinan, D. L. Osborne, J. Kimball, C. Chaston, J. McFadden, G. Delory, M. Temerin, and C. W. Carlson (1998), Aircraft observations conjugate to FAST: Auroral arc thicknesses, *Geophys. Res. Lett.*, *25*(12), 2073–2076, doi:10.1029/98GL01058.
Tanaka, T. (1994), Finite volume TVD scheme on an unstructured grid system for three-dimensional MHD simulation of inhomogeneous systems including strong background potential fields, *J. Comput. Phys.*, *111*, 381, doi:10.1006/jcph.1994.1071.
Tanaka, T. (2007), Magnetosphere-ionosphere convection as a compound system, *Space Sci. Rev.*, *133*, 1–72, doi:10.1007/s11214-007-9168-4.
Tanaka, T., A. Nakamizo, A. Yoshikawa, S. Fujita, H. Shinagawa, H. Shimazu, T. Kikuchi, and K. K. Hashimoto (2010), Substorm convection and current system deduced from the global simulation, *J. Geophys. Res.*, *115*, A05220, doi:10.1029/2009JA014676.
Untiedt, J., and W. Baumjohann (1993), Studies of polar current systems using the IMS Scandinavian magnetometer array, *Space Sci. Rev.*, *63*, 245–390, doi:10.1007/BF00750770.
Vasyliunas, V. M. (1984), Fundamentals of current description, in *Magnetospheric Currents*, edited by T. A. Potemra, AGU, Washington, D. C. doi:10.1029/GM028p0063.
Weygand, J. M., R. L. McPherron, H. Frey, O. Amm, K. Kauristie, A. T. Viljanen, and A. Koistinen (2008), Relation of substorm onset to Harang discontinuity, *J. Geophys. Res.*, *113*, A04213, doi:10.1029/2007JA012537.
Xing, X., L. R. Lyons, Y. Nishimura, V. Angelopoulos, E. Donovan, E. Spanswick, J. Liang, D. Larson, C. Carlson, and U. Auster (2011), Near-Earth plasma sheet azimuthal pressure gradient and associated auroral development soon before substorm onset, *J. Geophys. Res.*, *116*, A07204, doi:10.1029/2011JA016539.
Yago, K., K. Shiokawa, K. Yumoto, D. G. Baishev, S. I. Solovyev, and F. J. Rich (2007), Simultaneous DMSP, all-sky camera, and IMAGE FUV observations of the brightening arc at a substorm pseudo-breakup, *Earth Planets Space*, *59*, 45.
Yao, Y., Y. Ebihara, and T. Tanaka (2015), Sudden pressure enhancement and tailward retreat in the near-earth plasma sheet: THEMIS observation and MHD simulation, *J. Geophys. Res. Space Physics*, *120*, 201–211, doi:10.1002/2014JA020482.
Yao, Z. H., et al. (2012), Mechanism of substorm current wedge formation: THEMIS observations, *Geophys. Res. Lett.*, *39*, L13102, doi:10.1029/2012GL052055.
Zesta, E., L. R. Lyons, and E. Donovan (2000), The auroral signature of Earthward flow burst observed in the magnetotail, *Geophys. Res. Lett.*, *27*(20), 3241–3244, doi:10.1029/2000GL000027.
Zesta, E., E. Donovan, L. Lyons, G. Enno, J. S. Murphree, and L. Cogger (2002), Two-dimensional structure of auroral poleward boundary intensifications, *J. Geophys. Res.*, *107*(A11), 1350, doi:10.1029/2001JA000260.
Zesta, E., L. Lyons, C.-P. Wang, E. Donovan, H. Frey, and T. Nagai (2006), Auroral poleward boundary intensifications (PBIs): Their two-dimensional structure and associated dynamics in the plasma sheet, *J. Geophys. Res.*, *111*, A05201, doi:10.1029/2004JA010640.
Zou, S., L. R. Lyons, C.-P. Wang, A. Boudouridis, J. M. Ruohoniemi, P. C. Anderson, P. L. Dyson, and J. C. Devlin (2009), On the coupling between the Harang reversal evolution and substorm dynamics: A synthesis of SuperDARN, DMSP, and IMAGE observations, *J. Geophys. Res.*, *114*, A01205, doi:10.1029/2008JA013449.